UNIVERSITY OF LEEDS

This is a repository copy of *Blueschist from the Mariana forearc records long-lived residence of material in the subduction channel*.

White Rose Research Online URL for this paper:
http://eprints.whiterose.ac.uk/148736/

Version: Accepted Version

**Article:**

Tamblyn, R, Zack, T, Schmitt, AK et al. (5 more authors) (2019) Blueschist from the Mariana forearc records long-lived residence of material in the subduction channel. Earth and Planetary Science Letters, 519. pp. 171-181. ISSN 0012-821X

https://doi.org/10.1016/j.epsl.2019.05.013

(c) 2019, Elsevier B.V. This manuscript version is made available under the CC-BY-NC-ND 4.0 license https://creativecommons.org/licenses/by-nc-nd/4.0/

**Reuse**

This article is distributed under the terms of the Creative Commons Attribution-NonCommercial-NoDerivs (CC BY-NC-ND) licence. This licence only allows you to download this work and share it with others as long as you credit the authors, but you can't change the article in any way or use it commercially. More information and the full terms of the licence here: https://creativecommons.org/licenses/

**Takedown**

If you consider content in White Rose Research Online to be in breach of UK law, please notify us by emailing eprints@whiterose.ac.uk including the URL of the record and the reason for the withdrawal request.

White Rose
university consortium
Universities of Leeds, Sheffield & York

eprints@whiterose.ac.uk
https://eprints.whiterose.ac.uk/

*Manuscript
Click here to view linked References

# Blueschist from the Mariana forearc records long-lived residence of material in the subduction channel

Tamblyn, R.[1], Zack, T.[1,2], Schmitt, A. K.[3], Hand, M.[1], Kelsey, D.[1], Morrissey, L.[4], Pabst, S.[5], Savov, I.P.[6]

[1] Department of Earth Sciences, University of Adelaide, Adelaide, Australia
[2] Department of Earth Sciences, University of Gothenburg, Gothenburg, Sweden
[3] Institut für Geowissenschaften, Universität Heidelberg, Germany
[4] School of Natural and Built Environments, University of South Australia, Adelaide, Australia
[5] BHP Billiton Iron Ore, Exploration, PO Box 655, Newman, WA 6753, Australia
[6] School of Earth and Environment, University of Leeds, Institute of Geophysics and Tectonics, UK
Corresponding author: Renée Tamblyn (renee.tamblyn@adelaide.edu.au)

**Highlights**

- Blueschist from serpentine mud volcano in Mariana forearc is ca. 50 Ma old
- The mineral assemblage records warm metamorphic conditions during IBM subduction initiation
- Blueschist rocks have resided in the subduction channel for at least 46 Ma

**Abstract**

From ca. 50 Ma to present, the western Pacific plate has been subducting under the Philippine Sea plate, forming the oceanic Izu-Bonin-Mariana (IBM) subduction system. It is the only known location where subduction zone products are presently being transported to the surface by serpentinite-mud volcanoes. A large serpentine mud "volcano" forms the South Chamorro Seamount and was successfully drilled by ODP during Leg 195. This returned mostly partially serpentinized harzburgites enclosed in serpentinite muds. In addition, limited numbers of small (1 mm–1 cm) fragments of rare blueschists were also discovered. U–Pb dating of zircon and rutile from one of these blueschist clasts give ages of 51.1 ± 1.2 Ma and 47.5 ± 2.0 Ma, respectively. These are interpreted to date prograde high-pressure metamorphism. Mineral equilibria modelling of the blueschist clast suggests the mineral assemblage formed at conditions of ~1.6 GPa and ~590 °C. We interpret that this high-pressure assemblage formed at a depth of ~50 km within the subduction channel and was subsequently exhumed and entrained into the South Chamorro serpentinite volcano system at depths of ~27 km. Consequently, we propose that the material erupted from the South Chamarro Seamount may be sampling far greater depths within the Mariana subduction system than previously thought. The apparent thermal gradient implied by the pressure–temperature modelling (~370 °C/GPa) is slightly warmer than that predicted by typical subduction channel numerical models and other blueschists worldwide. The age of the blueschist suggests it formed during the arc initiation stages of the proto-Izu-Bonin-Mariana arc, with the P–T conditions recording thermally elevated conditions during initial stages of western Pacific plate subduction. This indicates the blueschist had prolonged residence time in the stable forearc as the system underwent east-directed rollback. The Mariana blueschist shows that subduction products can remain entrained in subduction channels for many millions of years prior to exhumation.

## 1. Introduction

From ca. 50 Ma until present, the Western Pacific plate has been subducting under the Philippine Sea plate, forming the oceanic Izu-Bonin-Mariana (IBM) arc-basin system (Figure 1; Stern and Bloomer, 1992; Ishizuka et al., 2011, 2018). This system provides an opportunity to study active processes within convergent intra-oceanic settings such as magmatism, seismicity, element recycling and hydrothermal transport. It is also the only known location on Earth where subduction zone products are actively transported to the surface by serpentinite-mud volcanoes (e.g. Fryer, 2012; Pabst et al., 2012). These serpentinite-mud volcanoes occur up to 90 km away from the trench axis in the forearc region (Figure 1; Fryer et al., 2006). In the southern Mariana segment, these volcanoes are interpreted to currently sample slab-generated fluids from a depth of up to 27 km (Fryer, 2012), offering a unique window into processes operating at shallow depths during subduction and in the mantle wedge above.

Previous studies on the variety of hard rock clasts “erupted” from these serpentinite-mud volcanoes have used them to infer the chemical and physical conditions of the subducting slab surface at shallow depths under the Mariana forearc (Savov et al., 2005; Fryer et al., 2006; Pabst et al., 2012). A major assumption from all previous studies is that the clasts and muds are derived from recently subducted products and hence are representative of the modern subduction system, however this assumption has never been tested. Additionally, there has been no in-depth and detailed metamorphic work done on the clasts to constrain the metamorphic conditions of formation and therefore the depth they sample within the subduction system. A high-pressure origin for blueschist clasts from the Mariana serpentinite-mud volcanoes has been suggested before, but never quantified (Maekawa et al., 1993; Fryer et al., 2006; Yamamoto et al., 1995). Because these metamorphic clasts contain a wealth of information about the thermal conditions within the slab, as well as potentially providing avenues to determine the age of metamorphic recrystallization, they can provide unique insights into the residence times of material within subduction channels formed by ocean-ocean plate convergence.

This study is focused on one mafic clast (195-1200E-1H-3-4b), recovered from serpentinite mud drilled during ODP Leg 195 at Site 1200 at the summit of the active South Chamorro Seamount (Figure 1; see Pabst et al. (2012) for further description on this sample). Clasts recovered from the drilling were predominately serpentinite fragments, however rare blueschist-facies metamafic fragments were also recovered. While multiple clasts contained blueschist-facies mineral assemblages (including amphibole, chlorite, epidote and phengite), one rare sample contained rutile and zircon which could be targeted for geochronology. We derive constraints on the thermobarometric conditions recorded by this sample, and the age of metamorphism. The results provide insight into the depth of material return to the surface, and the subduction channel P–T conditions during the very beginning of Mariana subduction.

## 2. Background

### 2.1 Geology and geometry of the IBM system

The IBM system is generated by the westward directed subduction of the Pacific oceanic plate under the Philippine Sea, which initiated at ca. 51 Ma (Figure 1; Reagan et al., 2010; Ishizuka et al., 2018). The northern IBM trench segment (Izu-Bonin) shows an increasing dip of the Wadati-Benioff zone from ~40° in the north to ~80° in the south, with intermediate-depth seismicity occurring between depths of ~150 to ~300 km (Gvirtzman and Stern, 2004). In contrast, the southern IBM segment (Mariana) has a subvertical Wadati-Benioff zone, with deep (>300 km) seismic events (Gvirtzman and Stern, 2004). As such, the width of the subduction zone interface between the overriding and subducting plates increases along the IBM from north to south (Gvirtzman and Stern, 2004). While this only delineates the current subduction zone structure under the IBM, it is useful for interpretations of subduction channel dynamics which presently operate. Currently, the slab in the Mariana segment is in a state of rollback, as the Pacific and Philippine plates are both advancing westwards, with the latter at a slightly faster rate (Gvirtzman and Stern, 2004). Complex geometries involving slab tearing and steepening in the southern segment of the IBM have led to the extreme dip and hence depth of the trench in this area (Gvirtzman and Stern, 2004). The Mariana forearc is extensively faulted, due to oblique convergence as well as the curvature produced by back-arc extension, resulting in it being dominated by sinistral shear (Stern et al., 2003). This structural architecture is probably a crucial factor in allowing serpentinized mantle to exhume and rise to the surface, driving serpentinite-mud volcanism. The Mariana forearc is the only place on modern Earth where this occurs (Fryer et al., 1992, 1999, 2000, 2006; Fryer, 2012;).

The recent history of the IBM is well studied. However, the cause for subduction inception in the IBM is the source of much debate, due to lack of access to the earliest subduction-generated rocks (e.g. Arculus et al., 2015; 2016). However, the Jurassic oceanic crust to the east formed a west-dipping subduction zone under the Philippine Sea or Pacific crust. The timing of this is estimated to be ca. 51–47 Ma (Ishizuka et al, 2011, 2018). Ar–Ar whole rock ages for initial construction of the Mariana arc match those for the Izu-Bonin arc at ca. 49–47 Ma, while forearc basement from the IBM has been dated by Ar–Ar to have formed by at least ca. 47–45 Ma (Cosca et al., 1998). More recently, the basement of the IBM arc was dated by Ar–Ar geochronology at 48.7 ± 0.3 Ma (Ishizuka et al., 2018). This age is further supported by nano and microfossils in the overlying volcaniclastic sediments (Arculus et al., 2015). A ca. 51 Ma age is reported based on stratigraphic relationships for tholeiitic fore-arc basalts interpreted to be the first lavas to erupt when the Pacific plate initially sunk under the Philippine plate (Reagan et al., 2010; 2017). This has been further supported by a U–Pb zircon age of 51.1 ± 1.5 from gabbro underlying the fore-arc basalts

(Ishizuka et al., 2011). Regardless of the exact timing of initiation, it seems that subduction initiation along the 2800 km IBM system occurred over 51–47 Ma (Stern et al., 2003; Arculus et al., 2015). The Kyushu-Palau Ridge (Figure 1) was active from ca. 48 Ma to ca. 25 Ma, and is the result of a stable magmatic arc during which the IBM subduction system was essentially immobile (Ishizuka et al., 2011). Spreading in the mid-southern Parece Vela Basin began after this (Figure 1a), and further spreading in the northern Izu-Bonin segment commenced at ca. 25 Ma with both terminating around 15 Ma due to collision of the northern IBM with Honshu (Stern et al., 2003). In the southern segment, eastwards rollback resulted in extension to form the Mariana Trough (~6 Ma back-arc basin), with the onset of seafloor spreading at ca. 3–4 Ma (Yamazaki and Stern, 1997). As such, the inception of the currently active Mariana Arc (Figure 1b; the West Mariana Ridge) is interpreted to be 3–4 Ma old (Stern et al., 2003), and the remnant arc was left behind. Over this Eocene–Pleistocene evolution, the relative slab rollback to the east has resulted in two former oceanic arcs younging from the Palau-Kyushu Ridge (active from the onset of subduction to ca. 25 Ma), to the current Mariana Ridge (Figure 1a).

### 2.2 Previous studies of blueschists from the Mariana forearc drill sites

A series of active mud volcanoes occur on the upper plate between the arc (the Mariana Ridge) and the Mariana Trough (current trench; Figure 1a). The two most intensely studied active seamounts are the South Chamorro Seamount and the Conical Seamount, which occur 85 and 90 km from the trench respectively (Fryer et al., 1999; Savov et al., 2005). Deep sea drilling of these serpentinite seamounts (ODP Legs 125 and 195) returned predominantly serpentinized harzburgite and dunite clasts, but also rare metabasic blueschist clasts (~5% of clasts) in a matrix of fine serpentinite muds (Savov et al., 2004; Fryer and Salisbury, 2006; Fryer et al., 2006). These clasts have been divided into amphibole-talc-chlorite-schists, chlorite-epidote-schists, amphibole-chlorite-phengite-schists and mono-mineralic aggregates of talc or amphibole (Pabst et al., 2012).

A variety of metamafic clasts as well as matrix serpentinite muds have been studied to make inferences about the pressure–temperature (P–T) conditions within and below the Conical and South Chamorro seamounts. Blueschist clasts were discovered during drilling of the Conical Seamount in the northern Mariana forearc (east of Asuncion; Figure 1b) by Maekawa et al. (1993), who reported the first direct evidence for low temperature and relatively high-pressure metamorphism in a subduction zone. These blueschists were estimated to have formed at temperatures of 150–250 °C and pressures of 5–6 kbar (potentially corresponding to depths of 16–20 km), based on the presence of aragonite, the compositions of sodic pyroxenes and temperature dependence of inferred metamorphic reactions (Maekawa et al., 1993). Maekawa et al. (1995) also noted the existence of lawsonite-bearing blueschist clasts, and indicated that higher grade metamorphic rocks may be sourced from below the seamount. Numerous blueschist clasts were recovered from Conical Seamount drilled during ODP Leg 125. These were analysed for their whole rock geochemistry by Yamamato et al. (1995), who concluded the volcano was returning clasts derived from a MORB source.

Blueschist clasts drilled from the summit of the South Chamorro Seamount to the east of Guam were recovered only recently (Figure 1b; Shipboard Scientific Party, 2000). Due to similar jadeitic (Jd) compositions of their pyroxenes, Pabst et al. (2012) estimated that blueschists from the South Chamorro Seamount had reached similar P–T conditions as those from Conical Seamount, studied by Maekawa et al. (1993; 1995). Further comparisons of the metamorphic mineral assemblages of the blueschists from South Chamorro Seamount with those of the Franciscan Complex have been used to infer conditions of 250–300 °C and 7 kbar for the late-stage blueschist facies assemblage (Pabst et al., 2012). Fryer et al. (2006) estimated conditions of ~250–300 °C and 4–5 kbar based on assumed equilibrium of epidote with magnesioriebeckite/barroisite from a different metabasite schist from South Chamorro Seamount. Higher grade conditions for metamorphic products have also been suggested by Murata et al. (2009) from the existence of antigorite in serpentinized peridotites. Antigorite coexisting with clinopyroxene and olivine indicates high-temperature serpentinization between ~450–550 °C, leading Murata et al., (2009) to suggest possible tectonic cycling of mantle wedge material. Additionally, temperatures and pressures of 350 °C and 8 kbar have been estimated for the source of serpentinite muds of the South Chamorro Seamount (Fryer et al., 2000), corresponding to depths of ~25–27 km. Fryer (1992) and Fryer et al. (2006) suggested that blueschists record higher grade conditions than those of the slab interface directly below the seamount, however no quantitative P–T estimates have been made. Geochemical and seismic studies, as well as earthquake locations on the subducting Pacific plate, have been used to suggest the mud volcanoes are sampling the slab interface at depth of 27–29 km (Oakley et al., 2008; Savov et al., 2005; Fryer et al., 2000). This is also generally supported by temperatures of ~200–300 °C estimated from chrysolite, lizardite and brucite-bearing serpentinized peridotites (D'Antonio and Kristensen, 2004). Fryer et al. (2006) suggested that MORB and OIB samples must have been derived from subducted oceanic plate buried to a depth of up to 30 km. This would suggest that the variety of clasts erupted from the South Chamorro Seamount and by inference other serpentinite volcanos in the Marianas forearc are being sampled from the slab interface beneath the volcano. While some of the geochemical signature of the fluid released from the South Chamorro Seamount appears to be originating from the currently subducting Pacific slab surface at a depth of ~27 km (Mottl et al., 2004), studies on the metamorphic conditions of the blueschist fragments span a range of P–T conditions.

In addition to the only limited constraints on the P–T conditions recorded by the metamorphic clasts, there is also lack of age data. While not overtly stated, existing studies on the mud hosted clasts assume they record modern conditions on the slab interface. However studies (Krebs et al., 2008; Lázaro et al., 2009; Blanco-Quintero et al., 2011) from high-pressure rocks in ancient serpentinite mélanges show that they may contain a range of metamorphic ages, indicating that material can reside within subduction zone channels for potentially tens of millions of years.

## 3. Methods

The ~ 2×2 mm blueschist clast recovered from ODP Site 1200 was mounted in epoxy resin and polished. It was primarily mapped in BSE using a Quanta 600 SEM at Adelaide Microscopy, University of Adelaide, using Mineral Liberation Analysis software, to determine petrological relationships and mineral modal proportions in the clast.

Quantitative Electron probe microanalysis (EPMA) elemental mapping used a CAMECA SXFive equipped with 5 wavelength-dispersive spectrometers (WDS) and X-Ray detectors, running the PeakSite software. Beam conditions were set at an accelerating voltage of 15 kV and 100 nA, utilising a focussed beam. Compositional mapping was done at a 4 µm pixel resolution. Pixel dwell time in all maps was set to 40 ms. Calibration and quantitative data reduction of maps was carried out with the "Probe for EPMA" software, distributed by Probe Software Inc. Calibration was performed on certified natural and synthetic standards from Astimex Ltd and P&H Associates. The clast was mapped for 10 elements using their Kα lines, thus requiring two mapping passes on the five spectrometers (Pass 1: Ca, Na, P, Mg, Fe; Pass 2: Ti, Si, Al, Mn, K). Potentially mobile elements were analysed in the first pass. The average minimum detection limits (at the 99% confidence interval) in wt.% for the quantitative maps were: Ca (0.06), Na (0.12), Ti (0.07), Mg (0.08), Fe (0.17), K (0.06), Si (0.01), P (0.08), Al (0.08), Mn (0.16).

The X-ray maps were then used to identify the metamorphic mineral assemblages and mineral modal proportions were determined by pixel counting using image analysis software. Although the blueschist clast contains some coarse-grained minerals, is generally medium-grained. As such, these modal proportions are reasonably representative of the local equilibrium volume. The modal proportion and electron microprobe compositions of mineral assemblages was used to compute a bulk chemical composition for petrological modelling (Supplementary Data Table 1). We chose this approach to determine a bulk composition as the sample was considered too valuable to be consumed for conventional-style geochemical analysis. Ti-magnetite was omitted from the bulk rock chemistry calculations, based on textural evidence it is magmatic. Allanite and zircon were also omitted as they contain elements that cannot be modelled. Results of pixel counting and associated calculations to construct the bulk composition are shown in Supplementary Data Table 2.

Mineral equilibria forward modelling was undertaken using THERMOCALC v 3.4 in the NCFMASHTO system, using the internally consistent thermodynamic dataset 'ds55' (filename tc-ds55.txt; November 2003 updated version of the Holland and Powell 1998 dataset) and activity–composition models in Diener et al. (2012) and references within. The calculated K and Mn concentrations in the calculated bulk rock composition are near zero, therefore K and Mn were excluded from the model system. Pumpellyite was not predicted in the modelling, possibly due to lack of a pumpellyite activity–composition model that allows solid solution. Calculations to test the sensitivity of modelled mineral equilibria to $H_2O$ content using P–$M_{H2O}$ models demonstrated the mineral assemblage, modal proportions and compositions recorded by the sample are stable over a large range of $H_2O$ contents (from 9 mol% to more than 13 mol %, Supplementary Figure 1). As a specific value could not be pinpointed, and the sample evidently formed under water-rich conditions as indicated by abundant chlorite, amphibole and epidote, modelling was done with water in excess, i.e. defining $H_2O$ as a saturating phase. Oxidation state ($Fe_2O_3$, or O in the bulk rock chemistry) was constrained from a P–$M_O$ model (Supplementary Figure 2), where mineral modal proportions and compositions overlapped in the interpreted peak field at approximately M(O) = 0.55, or O = 1.97 mol%. This value directly overlaps with recalculated mineral microprobe chemical analyses used to calculate the bulk rock chemistry by assuming perfect mineral stoichiometry in the calculation of cations from the wt% oxide data (Droop, 1987; Leake et al., 1997). Contouring of the mineral equilibria model for the normalised abundances (mode) of minerals was calculated using the software TCInvestigator v1.0 (Pearce et al., 2015).

Secondary ionization mass spectrometry (SIMS) U-Pb geochronology was carried out using a CAMECA ims 1270 ion microprobe at the University of California of Los Angeles (Supplementary Data Table 3). In-situ analyses targeted zircon in the polished blueschist block using methods for analysis of small grains in their matrix as described in Schmitt et al. (2010).

Rutile analyses were also performed in situ on the same mount, but due to the larger grain size of rutile compared to zircon, nearly full transmission was reached in the ion microprobe's field aperture. Instrumental set-up for rutile analysis is summarized in Schmitt and Zack (2012); all ages are reported relative to AS3 reference zircon (1099 Ma; Paces and Miller, 1993) and R10b reference rutile (1090 Ma; Luvizotto et al., 2009).

## 4. Results

### 4.1 Petrography

The blueschist clast (E1H3-4b) is dominated by an amphibole and chlorite-bearing matrix, with less abundant epidote, rutile, titanite and allanite, and very rare pumpellyite, phengite and clinopyroxene (Figure 2). Amphibole is typically ~10–>200 μm in size and zoned (Figure 3; 4), with patchy magnesio-hornblende cores, surrounded by volumetrically dominant edenite/pargasite, and then a sharply-defined thin rim of magnesiokatophorite (Figure 5a, nomenclature follows Leake et al., 1997). This zonation can be seen in element maps (Figure 4a), with a marked increase in Na and Fe from core to rim, a decrease in Mg and Ca from core to rim, and high $SiO_2$ cores and rims and corresponding low alumina cores and rims. Small needle-like grains of actinolite also occur within the amphibole. Chlorite is commonly usually less than 50 μm, but rare grains are up to 300 μm in size. It is weakly zoned with thin rims that are comparatively poor in Fe and Al but rich in Si and Mg (Figure 3b, Figure 5b). It forms irregular grains intergrown with amphibole and epidote as well as narrow veins which cross-cut or occur along amphibole cleavage planes. Epidote occurs as smaller (occasionally up to ~250 μm) grains within amphibole or chlorite. It regularly overgrows texturally early allanite (Figure 2), and is unzoned, except for a thin rim of elevated Fe (Figure 5c, increase of ~1.65 wt% $Fe_2O_3$; Supplementary Data Table 1). Allanite is up to 80 μm in size and oscillatory zoned in rare earth elements (Figure 2), consistent with metamorphic allanite grown in the presence of fluid. Ti-magnetite (~10–100 μm) is overgrown by rims of rutile (up to ~100 μm across). Titanite forms discontinuous overgrowths on the rutile and

Ti-magnetite which are up to 40 μm wide (Figure 2), and also occurs as euhedral crystals with amphibole and chlorite. Minor (<1%) fine-grained (5–20 μm) pumpellyite is associated with retrograde titanite and chlorite. Rare fine-grained clinopyroxene (<10 μm) occurs in the chlorite-amphibole matrix, and contains 7–26 mol% jadeite (Figure 5d, Pabst et al., 2012). Very fine-grained rare phengite occurs as needles in amphibole, and fine-grained zircon up to 10 μm also occurs in amphibole and epidote. The main mineral assemblages are: 1) early Na-rich amphibole core, chlorite, epidote, clinopyroxene and rutile, and 2) late Na-Fe rich amphibole rims, actinolite, titanite, and pumpellyite. Quartz is absent, and is typically absent from most blueschists from South Chamorro (Pabst et al., 2012).

### 4.2 Zircon and rutile geochronology

Textually resolved in-situ SIMS U–Pb geochronology (Figure 6) yields concordia ages of 47.5 ± 2.0 Ma (mean square of weighted deviates MSWD of concordance = 0.00052; n = 9) for rutile, and 51.1 ± 1.2 Ma (MSWD = 0.16; n = 4) for zircon (Figure 7; Supplementary Data Table 3). U abundances in rutile range between 11 and 30 ppm, and corresponding radiogenic $^{206}$Pb yields are between 42 and 95%. U abundances in zircon range from ~180 to ~1300 ppm, with high radiogenic $^{206}$Pb yields of >97% in favourable cases. Zirconium in rutile has on average 380 ppm, which corresponds in the presence of zircon and absence of quartz to a maximum temperature of 650 °C using the Tomkins et al. (2007) calibration at pressures 1.5 GPa derived from mineral equilibria modelling (see below).

### 4.3 Mineral equilibria modelling

A peak to retrograde P–T evolution can be inferred from the compositional isopleths of amphibole as well as the modal proportions of metamorphic minerals for the modelled mineral equilibria (Supplementary Data Table 2; Figure 8; in one-oxide-normalized %, compliant with the modes computed by THERMOCALC). Uncertainties on the calculations in the mineral equilibria model are 2 sigma and are shown in Supplementary Figure 3. The peak assemblage consists of chlorite +

amphibole + epidote + clinopyroxene (diopside) + rutile, and is bound by the disappearance of clinopyroxene and the addition of hematite to higher temperatures, and the solid-solution transition of diopside to omphacite (across the clinopyroxene solvus) at lower temperatures and higher pressures. The peak assemblage occurs over a large range of conditions, from 1.1 ± 0.07 GPa and 515 ± 9 °C to 1.8 ± 0.06 GPa and 600 ± 21 °C. The retrograde evolution is characterized by the formation of titanite and calcic amphibole, evidenced by the presence of titanite coronas on rutile and small, late actinolite needles within amphibole. Clinopyroxene is interpreted to be relict from the peak assemblage, and therefore the retrograde path also involves the loss of clinopyroxene. The P–T path can be further constrained using amphibole compositional isopleths. Compositional parameters A (xNa on the A site), C (xCa on the M4 site) and Z (xNa on the M4 sites) were calculated from amphibole microprobe data and plotted on the mineral equilibria model (grey dashed lines). Compositional isopleths of the amphibole cores plot over a wide range of pressures and temperatures, from 1.2–1.7 GPa and 540–600 °C, with average errors on each compositional range of ± 0.07 GPa and 12 °C. Corresponding model proportions of the amphibole cores from 1.5–1.7 (± 0.06) GPa and 575–600 (± 12) °C. Although not definitive, it is likely the compositions and modal proportions of the magnesio-hornblende cores point to a high-pressure history that predated the formation of the texturally dominant assemblage in the rock. Modal proportion isopleths of chlorite, total amphibole and epidote within the modelled peak field span from 1.1–1.45 GPa and 540–590 °C with average errors of 0.07 GPa and 10 °C, and also occur in retrograde P–T space with the addition of titanite. The compositions of amphibole rims (magnesiokatophorite) plot within the field of the retrograde mineral assemblage from 0.7–0.9 GPa and 470–495 °C, with average errors of 0.06 GPa and 9 °C.

### 4.4 Protolith constraints

The investigated sample has an unusual whole rock composition, with 44.2 mol% SiO2 and 22 mol% MgO (Supplementary Data Table 2). Technically it can be labelled a picrite, which is not typically observed in likely protoliths such as MORB, OIB or former arc basement. A more realistic scenario to explain the bulk rock composition is the formation of a hybrid rock composition derived from MORB with a metasomatic imprint from surrounding hydrated mantle, similar to that observed on Catalina Island (e.g. Bebout and Barton 2002; Pabst et al., 2012). The implication is that the investigated sample was not part of a coherent subducting slab at the time of zircon and rutile formation.

## 5. Discussion

Texturally, rutile in blueschist clast E1H3-4b forms part of a typical high-pressure metamorphic assemblage (Zack & Kooijman, 2017). Furthermore rutile is extremely rare as an igneous mineral in mafic rocks, and the chance that the erupted clast sampled a metamorphosed mafic rock with relic igneous rutile would appear negligible. Zircon is relatively common in mafic subvolcanic and plutonic rocks as a late-crystallizing igneous mineral, however in general it is not abundant in MORB. A magmatic zircon age from crystallisation of the subducting slab for the zircon can probably be dismissed as the age of oceanic crust being subducted into the IBM system is Jurassic (Stern et al., 2003). Moreover, the similarity in age to the rutile also strongly implies a metamorphic origin. Hence, the U–Pb ages from rutile and zircon are interpreted to record the high-pressure metamorphism.

Texturally, rutile rims early magmatic Ti-magnetite (Figure 6a). Regardless of the P–T path taken by the clast, rutile growth would have occurred on the prograde path (Figure 8), and continued to be stable to the peak conditions. To demonstrate this, black dashed lines on the mineral equilibria model indicate the stabilization of rutile (rutile in) and the maximum rutile mode reached (Figure 8a), after this mode line rutile abundance is unchanging as it does not continue to grow. As the closure temperature of U–Pb diffusion in rutile is estimated to be ca. 600–640 °C (Zack & Kooijman 2017), the age of ca. 47.5 Ma most likely represents the growth of rutile during prograde metamorphism.

The mechanism of metamorphic zircon formation in low-temperature metamorphic rocks is still not well understood. Zircon occurs in the clast as small (5–50 µm) euhedral grains within matrix amphibole and epidote/allanite (Figure 6b,c). Metamorphic zircon in blueschist-facies mafic rocks is thought to grow as a result of either dissolution-precipitation of inherited zircon, or release of zirconium through the breakdown of higher temperature minerals such as magmatic pyroxene (e.g. Rubatto and Hermann, 2007) and granulite-facies rutile (Zack & Kooijman 2017). There is no evidence for relic inherited zircon or textural features suggesting dissolution-precipitation (Rubatto and Hermann, 2007; Rubatto et al., 2008). Possible mechanisms of zircon growth in the sample are the breakdown of Zr-bearing magmatic minerals which persisted to high pressures (Rubatto and Hermann, 2007). Breakdown of Ti-magnetite to form zircon (+ rutile + Fe-phase) on the prograde path would result in both minerals producing similar ages as they were formed in the same reaction. Alternatively, breakdown of magmatic clinopyroxene to amphibole also may release zirconium, and may have been the source during prograde metamorphism (Rubatto et al., 2008). While the exact prograde reaction that formed zircon is unclear, the closure temperature of U–Pb diffusion in zircon is estimated to be >900 °C (Cherniak and Watson, 2001). Therefore, the Eocene age is interpreted to record growth of zircon during metamorphism that occurred very soon after subduction initiation.

The mineral equilibria modelling results indicate a peak to retrograde evolution from ~ 1.6 GPa to 0.8 GPa. Although the exact P–T points are poorly constrained, the path is strongly supported by textural relationships within the sample, mineral modal proportions, and the compositions of zoned amphibole. It is possible to suggest a higher-pressure peak assemblage at approximately 1.6 ± 0.2 GPa and 585 ± 20 °C, followed by a retrograde evolution towards ~ 0.8 ± 0.15 GPa and 485 ± 30 °C. These conditions range in approximate apparent thermal gradients from ~ 370 °C/GPa at peak, and ~ 600 °C/GPa during the retrograde evolution, with an average of around 470 °C/GPa. These approximations could be within error of uncertainties within the mineral equilibria model

(Supplementary Figure 1), and the geochronology from the clast only constrains the prograde part of this evolution. However, if it is not within error of the mineral equilibria model uncertainties, the change in thermal gradient may reflect changes in subducting slab geometry, as the slab becomes steeper at greater depth, resulting in lower thermal gradients at depth (Peacock, 2003; Syracuse et al, 2010; Penninston-Dorland et al., 2015). Alternatively, the change in thermal gradient could be due to the advection of heat within the rising serpentinite melange that carried the blueschist clast to comparatively shallow depths within the subduction channel (Gerya et al., 2002). These pressure-temperature conditions are in line with measured global subduction zone data (Figure 9a,b,c; Penniston-Dorland et al., 2015; Brown and Johnson, 2017; Agard et al., 2018), albeit slightly above the global average. When compared to numerical models (Figure 9d; Gerya et al., 2002; Syracuse et al., 2010; van Keken et al., 2011; Ruh et al., 2018), the pressure-conditions remain slightly above average, all though this may be due to the exclusion of shear heating as a model parameter (e.g. Kohn et al., 2018). Combined with the U–Pb rutile and zircon geochronology, the P–T data suggests the blueschist clast records initially warm conditions relative to global norms during the early initiation of subduction of the Pacific plate (ca. 52 Ma; Ishizuka et al., 2011; 2018; Agard et al., 2018). During the early stages of subduction, conditions are generally warmer, as the plate subducts at a shallower angle, and the 'dragging down' of geotherms at the base of the overlying mantle wedge has not yet been significantly achieved (Gerya et al., 2002). 'Warm' pressure-temperature estimates from newly initiated subduction zones have also been recorded by high-pressure mafic rocks (Figure 9c; Agard et al., 2018).

Forearc and reararc basalts mark the initiation of subduction in the Mariana system, and are immediately followed by forearc boninite magmatism from 48.2–45.1 Ma (Reagan et al., 2008; Ishuzuka et al., 2011; Arculus et al., 2015; Reagan et al., 2017). The eruption of these boninites necessitates the interaction of very depleted mantle wedge with slab-derived fluids at shallow depths during subduction, and was coeval with blueschist metamorphism (this study). The similarity between the metamorphic ages obtained in this study and the age of boninitic magmatism, as well as the higher than usual thermal gradients recorded by the mineral assemblage, supports the existence of a hot mantle wedge above a warm subduction channel during early stages of subduction initiation in the Marianas.

If only lithostatic pressure is assumed, then the pressure estimates correspond to depths ranging from ~46 km to ~25 km. Therefore, it appears the retrograde P–T path essentially ends at conditions corresponding to the slab depth below the South Chamorro Seamount (~27 km; Pabst et al., 2012; Fryer et al., 2006). ODP Site 1200 is on the summit of the seamount (Figure 1b; Shipboard Scientific Party, 2000), and therefore it can be assumed that the drill core represents most recent mud extrusions from the serpentinite-mud volcano (Fryer et al., 2006). The oldest magmatic volcanism in the current Mariana arc (or Mariana ridge, Figure 1b) is interpreted to be ca. 3–4 Ma (Stern et al., 2003), and as such the position of the subduction zone and the maximum age of the serpentinite volcanoes is reasonably inferred as being similar. However, the rutile and zircon ages record metamorphism at ca. 50 Ma. This suggests that the clast was trapped somewhere within the subduction channel for at least ca. 46 Ma. The preservation of mineral assemblages that record ‘warm’ peak metamorphic conditions, as well as metamorphic rutile and zircon with Eocene ages, can be explained by either residence at peak depths for a significant portion of the metamorphic history of the clast, or that this clast was exhumed to shallower depths under the forearc and resided at cool conditions where recrystallization of minerals to lower pressure-temperature assemblages was not achieved. Unfortunately, there are no geochronologic constraints on when the blueschist was exhumed from depth to distinguish between these possibilities. The lack of retrograde recrystallisation may suggest that the small clast was protected from fluids and may have been armoured within a larger blueschist boudin or ‘knocker’, as commonly occur in high-pressure metamorphic and serpentinite mélanges such as the Franciscan Complex and Carribean (cf. Becker and Cloos, 1985; Lázaro et al., 2009; Blanco-Quintero et al., 2011). While the lack of geochronology on the retrograde history of the rock precludes definite explanation, it seems likely that the clast was exhumed to a shallow refrigerated region under the forearc in the Mariana subduction channel some time between ca 49 and 3 Ma, prior to its eruption in the mud volcano (Figure 10). However, the exact mechanism of this exhumation from ca. 50 km deep remains unknown. It could have occurred as return flow of the hydrated serpentinite mantle wedge cycled high-pressure material as the Mariana subduction system matured and steepened (Gerya et al., 2002). Alternatively, detachment and slicing of oceanic crust within the subduction channel could have allowed partial exhumation of the blueschist-facies material (Ruh et al., 2015; Agard et al., 2018). Regardless, given that the clast is erupted in a serpentinite-mud volcano, serpentinite-driven buoyancy appears to have been an important part of the exhumation mechanism.

Implicit in the above scenario is that the blueschist must have formed during the early stages of subduction under the proto-IBM arc. A number of workers (e.g. Cosca et al., 1988; Reagan et al., 2008; 2010; Ishizuka et al., 2018), have argued that subduction initiated at around 51–47 Ma ago. High-pressure metamorphism at ca. 50 Ma supports the upper scale of those scenarios. The current location of the trench is ~ 1300 km to the east of the ridge (Figure 1a), as slab rollback has resulted in extension of the Philippine Sea Plate. This means that the forearc not only entrapped and preserved the blueschist clast, but it also survived at least partly intact in its ~1300 km long eastward journey transported by slab rollback. A similar scenario has been suggested for long-lived (>40 Ma) entrapment of high-pressure metamorphic rocks in serpentinite mélange in other oceanic subduction systems such as the Caribbean and the Franciscan Complex (Krebs et al., 2008; Lázaro et al., 2009; Blanco-Quintero et al., 2011).

The age and source region of the blueschist clast sampled from the South Chamorro seamount has implications for interpretations and future models regarding subduction zone conditions inferred from past studies on erupted clasts and muds from these seamounts. Some authors (Fryer et al., 1992; Savov et al., 2005; Fryer et al., 2006; Murato et al., 2009), have indicated that subduction products from serpentinite volcanoes may be sampled from greater depths than the slab immediately below the mud volcano and therefore have more complex source regions. However, they have been unable to quantify those depths. These authors have also assumed that the material exhumed in the mud volcanism was recently subducted.  As such, the data has been used to describe ongoing Mariana trench subduction systematics, when in fact the subduction zone retains an integration of material from its inception until recently. The inferred depth from the modelled metamorphic assemblage in the blueschist clast indicates that the ‘plumbing system’ of the Marianas mud volcanoes is much more temporally and spatially complex than previously thought, meaning the metamorphic clasts in the IBM mud volcanoes capture a long history of the chemical and thermal evolution of the western Pacific slab. This temporally and spatially complex range of sources for material from the mud volcanoes means that caution should be exercised when interpreting data from clasts or muds erupted from seamounts in the Mariana forearc.

## 6. Conclusions

Detailed petrographic analyses and mineral equilibria forward modelling of a blueschist clast from the South Chamorro Seamount in the Mariana forearc indicates the mud volcano samples material from depths of ca. 50 km, which is well below the current depth of the slab directly below the volcano. The modelled P–T conditions (ca. 1.6 GPa and 590 °C) of the blueschist clast indicate the thermal regime was warmer than typical oceanic subduction, suggesting the modelled mineral assemblage formed in the initial stages of the IBM subduction system. This is consistent with concordant U–Pb ages of ca. 50 Ma from rutile and zircon within the blueschist assemblage, confirming the mineral assemblage formed soon after the Pacific plate began subducting under the Philippine Sea plate. Maturation of the subduction zone and formation of serpentinite within the subduction channel then facilitated return flow, driving exhumation of the blueschist clast to a refrigerated region under the forearc for at least ca. 46 Ma, before it was erupted in the South Chamorro mud volcano in the Mariana forearc. During this period of time there was ~1300 km of east-directed slab rollback, which transported the blueschist and other early subduction products with it. Therefore the South Chamorro Seamount, and by inference other volcanoes in the Mariana forearc, are probably sampling a temporally and spatially diverse range of lithologies and P–T–t histories that document the thermal evolution of the surface of the subducting plate over time. The data from the Mariana system suggests that potential serpentinite hosted blueschist and eclogite blocks in ancient subduction product complexes (e.g. Franciscan and Caribbean) may hold extensive records of the thermal evolution of subducting slabs.

**Acknowledgements**

We would like to thank Ben Wade of Adelaide Microscopy for his assistance running element maps. We also thank E. Baxter and P. Agard for their thoughtful reviews, and M. Bickle for his editorial handling. This work was supported by ARC grant DP160104637 and DFG grant Za285/4. The ion microprobe facility at UCLA is partly supported by a grant from the Instrumentation and Facilities Program, Division of Earth Sciences, National Science Foundation.

## References

Agard, P., Plunder, A., Angiboust, S., Bonnet, G., & Ruh, J. (2018). The subduction plate interface: Rock record and mechanical coupling (from long to short time scales). Lithos.

Arculus, R. J., Ishizuka, O., Bogus, K. A., Gurnis, M., Hickey-Vargas, R., Aljahdali, M. H., . . . Drab, L. (2015). A record of spontaneous subduction initiation in the Izu-Bonin-Mariana arc. Nature Geoscience, 8(9), 728-733.

Arculus, R. J., Ishizuka, O., Bogus, K. A., Gurnis, M., Hickey-Vargas, R., Aljahdali, M. H., . . . Drab, L. (2016). Reply to'Unclear causes for subduction'. Nature Geoscience, 9(5), 338.

Bebout, G. E., & Barton, M. D. (1993). Metasomatism during subduction: products and possible paths in the Catalina Schist, California. Chemical Geology, 108(1-4), 61-92.

Becker, D. G., & Cloos, M. (1985). Mélange diapirs into the Cambria Slab: A Franciscan trench slope basin near Cambria, California. The Journal of Geology, 93(2), 101-110.

Blanco-Quintero, I. F., García-Casco, A., & Gerya, T. V. (2011). Tectonic blocks in serpentinite mélange (eastern Cuba) reveal large-scale convective flow of the subduction channel. Geology, 39(1), 79-82.

Brown, M., & Johnson, T. (2018). Secular change in metamorphism and the onset of global plate tectonics. American Mineralogist, 103(2), 181-196.

Cherniak, D., & Watson, E. (2001). Pb diffusion in zircon. Chemical Geology, 172(1), 5-24.

Cosca, M., Arculus, R. J., Perace, J., & Mitchell, J. G. (1998). 40Ar/39Ar and K–Ar geochronological age constraints for the inception and early evolution of the Izu–Bonin–Mariana arc system. Island Arc, 7(3), 579-595.

D’antonio, M., & Kristensen, M. (2004). Serpentine and brucite of ultramafic clasts from the South Chamorro Seamount (Ocean Drilling Program Leg 195, Site 1200): inferences for the serpentinization of the Mariana forearc mantle.

Diener, J., & Powell, R. (2012). Revised activity–composition models for clinopyroxene and amphibole. Journal of metamorphic Geology, 30(2), 131-142.

Droop, G. (1987). A general equation for estimating Fe3+ concentrations in ferromagnesian silicates and oxides from microprobe analyses, using stoichiometric criteria. Mineralogical Magazine, 51(361), 431-435.

Fryer, P. (2012). Serpentinite mud volcanism: observations, processes, and implications. Annual review of marine science, 4, 345-373.

Fryer, P., Gharib, J., Ross, K., Savov, I., & Mottl, M. (2006). Variability in serpentinite mudflow mechanisms and sources: ODP drilling results on Mariana forearc seamounts. Geochemistry, Geophysics, Geosystems, 7(8).

Fryer, P., Lockwood, J. P., Becker, N., Phipps, S., & Todd, C. S. (2000). Significance of serpentine mud volcanism in convergent margins. SPECIAL PAPERS-GEOLOGICAL SOCIETY OF AMERICA, 35-52.

Fryer, P., Pearce, J., & Stokking, L. (1992). 36. A synthesis of Leg 125 drilling of serpentine seamounts on the Mariana and Izu–Bonin forearcs. Paper presented at the Proceedings of the Ocean Drilling Program, Scientific Results.

Fryer, P., & Salisbury, M. (2006). Leg 195 synthesis: Site 1200-Serpentinite seamounts of the Izu-Bonin/Mariana convergent plate margin (ODP Leg 125 and 195 drilling results). Paper presented at the Proc. ODP, Sci. Results.

Fryer, P., Wheat, C., & Mottl, M. (1999). Mariana blueschist mud volcanism: Implications for conditions within the subduction zone. Geology, 27(2), 103-106.

Gerya, T. V., Stöckhert, B., & Perchuk, A. L. (2002). Exhumation of high- pressure metamorphic rocks in a subduction channel: A numerical simulation. Tectonics, 21(6).

Gvirtzman, Z., & Stern, R. J. (2004). Bathymetry of Mariana trench- arc system and formation of the Challenger Deep as a consequence of weak plate coupling. Tectonics, 23(2).

Holland, T., & Powell, R. (1998). An internally consistent thermodynamic data set for phases of petrological interest. Journal of metamorphic Geology, 16(3), 309-343.

Ishizuka, O., Hickey-Vargas, R., Arculus, R. J., Yogodzinski, G. M., Savov, I. P., Kusano, Y., . . . Sudo, M. (2018). Age of Izu–Bonin–Mariana arc basement. Earth and Planetary Science Letters, 481(Supplement C), 80-90. doi: https://doi.org/10.1016/j.epsl.2017.10.023

Ishizuka, O., Tani, K., Reagan, M. K., Kanayama, K., Umino, S., Harigane, Y., . . . Dunkley, D. J. (2011). The timescales of subduction initiation and subsequent evolution of an oceanic island arc. Earth and Planetary Science Letters, 306(3), 229-240.

Krebs, M., Maresch, W., Schertl, H.-P., Münker, C., Baumann, A., Draper, G., . . . Trapp, E. (2008). The dynamics of intra-oceanic subduction zones: a direct comparison between fossil petrological evidence (Rio San Juan Complex, Dominican Republic) and numerical simulation. Lithos, 103(1), 106-137.

Lázaro, C., García- Casco, A., Rojas Agramonte, Y., Kröner, A., Neubauer, F., & ITURRALDE- VINENT, M. (2009). Fifty- five- million- year history of oceanic subduction and exhumation at the northern edge of the Caribbean plate (Sierra del Convento mélange, Cuba). Journal of metamorphic Geology, 27(1), 19-40.

Leake, B. E., Woolley, A. R., Arps, C. E., Birch, W. D., Gilbert, M. C., Grice, J. D., . . . Krivovichev, V. G. (1997). Report. Nomenclature of amphiboles: report of the subcommittee on amphiboles of the international mineralogical association commission on new minerals and mineral names. Mineralogical Magazine, 61(2), 295-321.

Luvizotto, G., Zack, T., Meyer, H., Ludwig, T., Triebold, S., Kronz, A., . . . Klemme, S. (2009). Rutile crystals as potential trace element and isotope mineral standards for microanalysis. Chemical Geology, 261(3-4), 346-369.

Maekawa, H., Fryer, P., & Ozaki, A. (1995). Incipient Blueschist- Facies Metamorphism in the Active Subduction Zone Beneath the Mariana Forearc. Active margins and marginal Basins of the Western pacific, 281-289.

Maekawa, H., Shozul, M., Ishll, T., Fryer, P., & Pearce, J. A. (1993). Blueschist metamorphism in an active subduction zone. Nature, 364(6437), 520-523.

Mottl, M. J., Wheat, C. G., Fryer, P., Gharib, J., & Martin, J. B. (2004). Chemistry of springs across the Mariana forearc shows progressive devolatilization of the subducting plate. Geochimica et Cosmochimica Acta, 68(23), 4915-4933.

Murata, K., Maekawa, H., Yokose, H., Yamamoto, K., Fujioka, K., Ishii, T., . . . Wada, Y. (2009). Significance of serpentinization of wedge mantle peridotites beneath Mariana forearc, western Pacific. Geosphere, 5(2), 90-104.

Oakley, A., Taylor, B., & Moore, G. (2008). Pacific Plate subduction beneath the central Mariana and Izu- Bonin fore arcs: New insights from an old margin. Geochemistry, Geophysics, Geosystems, 9(6).

Pabst, S., Zack, T., Savov, I. P., Ludwig, T., Rost, D., Tonarini, S., & Vicenzi, E. P. (2012). The fate of subducted oceanic slabs in the shallow mantle: insights from boron isotopes and light element composition of metasomatized blueschists from the Mariana forearc. Lithos, 132, 162-179.

Paces, J. B., & Miller, J. D. (1993). Precise U- Pb ages of Duluth complex and related mafic intrusions, northeastern Minnesota: Geochronological insights to physical, petrogenetic, paleomagnetic, and tectonomagmatic processes associated with the 1.1 Ga midcontinent rift system. Journal of Geophysical Research: Solid Earth, 98(B8), 13997-14013.

Peacock, S. M. (2003). Thermal structure and metamorphic evolution of subducting slabs. Inside the subduction factory, 7-22.

Pearce, M., White, A., & Gazley, M. (2015). TCInvestigator: automated calculation of mineral mode and composition contours for thermocalc pseudosections. Journal of metamorphic Geology, 33(4), 413-425.

Penniston-Dorland, S. C., Kohn, M. J., & Manning, C. E. (2015). The global range of subduction zone thermal structures from exhumed blueschists and eclogites: Rocks are hotter than models. Earth and Planetary Science Letters, 428, 243-254.

Reagan, M. K., Hanan, B. B., Heizler, M. T., Hartman, B. S., & Hickey-Vargas, R. (2008). Petrogenesis of volcanic rocks from Saipan and Rota, Mariana Islands, and implications for the evolution of nascent island arcs. Journal of Petrology, 49(3), 441-464.

Reagan, M. K., Ishizuka, O., Stern, R. J., Kelley, K. A., Ohara, Y., Blichert- Toft, J., . . . Hanan, B. B. (2010). Fore- arc basalts and subduction initiation in the Izu- Bonin- Mariana system. Geochemistry, Geophysics, Geosystems, 11(3).

Reagan, M. K., Pearce, J. A., Petronotis, K., Almeev, R. R., Avery, A. J., Carvallo, C., . . . Godard, M. (2017). Subduction initiation and ophiolite crust: new insights from IODP drilling. International Geology Review, 59(11), 1439-1450.

Rubatto, D., & Hermann, J. r. (2007). Zircon behaviour in deeply subducted rocks. Elements, 3(1), 31-35.

Rubatto, D., Müntener, O., Barnhoorn, A., & Gregory, C. (2008). Dissolution-reprecipitation of zircon at low-temperature, high-pressure conditions (Lanzo Massif, Italy). American Mineralogist, 93(10), 1519-1529.

Ruh, J. B., Le Pourhiet, L., Agard, P., Burov, E., & Gerya, T. (2015). Tectonic slicing of subducting oceanic crust along plate interfaces: Numerical modeling. Geochemistry, Geophysics, Geosystems, 16(10), 3505-3531.

Savov, I., Tonarini, S., Ryan, J., & Mottl, M. (2004). Boron isotope geochemistry of serpentinites and porefluids from Leg 195, Site 1200, S. Chamorro Seamount, Mariana forearc region. Paper presented at the International Geological Congress (IGC), Florence, Italy.

Savov, I. P., Ryan, J. G., D'Antonio, M., Kelley, K., & Mattie, P. (2005). Geochemistry of serpentinized peridotites from the Mariana Forearc Conical Seamount, ODP Leg 125: Implications for the elemental recycling at subduction zones. Geochemistry, Geophysics, Geosystems, 6(4).

Schmitt, A. K., Stockli, D. F., Lindsay, J. M., Robertson, R., Lovera, O. M., & Kislitsyn, R. (2010). Episodic growth and homogenization of plutonic roots in arc volcanoes from combined U–Th and (U–Th)/He zircon dating. Earth and Planetary Science Letters, 295(1-2), 91-103.

Schmitt, A. K., & Zack, T. (2012). High-sensitivity U–Pb rutile dating by secondary ion mass spectrometry (SIMS) with an O2+ primary beam. Chemical Geology, 332, 65-73.

Stern, R. J., & Bloomer, S. H. (1992). Subduction zone infancy: examples from the Eocene Izu-Bonin-Mariana and Jurassic California arcs. Geological Society of America Bulletin, 104(12), 1621-1636.

Stern, R. J., Fouch, M. J., & Klemperer, S. L. (2003). An overview of the Izu‐ Bonin‐ Mariana subduction factory. Inside the subduction factory, 175-222.

Syracuse, E. M., van Keken, P. E., & Abers, G. A. (2010). The global range of subduction zone thermal models. Physics of the Earth and Planetary Interiors, 183(1-2), 73-90.

Tomkins, H., Powell, R., & Ellis, D. (2007). The pressure dependence of the zirconium‐ in‐ rutile thermometer. Journal of metamorphic Geology, 25(6), 703-713.

van Keken, P. E., Hacker, B. R., Syracuse, E. M., & Abers, G. A. (2011). Subduction factory: 4. Depth‐ dependent flux of H2O from subducting slabs worldwide. Journal of Geophysical Research: Solid Earth, 116(B1).

Yamamoto, K., Asahara, Y., Maekawa, H., & Sugitani, K. (1995). Origin of blueschist-facies clasts in the Mariana forearc, Western Pacific. Geochemical Journal, 29(4), 259-275.

Yamazaki, T., & Stern, R. J. (1997). Topography and magnetic vector anomalies in the Mariana Trough. JAMSTEC J. Deep Sea Res, 13, 31-45.

Zack, T., & Kooijman, E. (2017). Petrology and geochronology of rutile. Reviews in mineralogy and geochemistry, 83(1), 443-467.

## Figure captions

**Figure 1.** a) Bathymetric map of the Mariana segment of the IBM system, showing the tectonic plates and ridges. Cross section is marked a' to b'. Location of South Chamorro Seamount is indicated in black arrow. Modified from Fryer et al. (2002). b) 3D bathymetric image of South Chamorro Seamount, indicated ODP drill site location after Savov et al (2005). c) Interpreted cross section (a'–b') of the Mariana trench and forearc. Vertical exaggeration is 2:1. Plate location and structure of the Philippine and Pacific plates after Fryer et al. (1999), Oakley et al. (2008) and Pabst et al. (2012). Schematic representation of serpentinisation after Ruh et al. (2015).

**Figure 2:** Mineralogical map of blueschist chip sample E1H3-4b, based on BSE imaging and X-ray derived elemental maps. C and R correspond to examples of amphibole cores and rims. Fine-grained minerals such as pumpellyite, clinopyroxene and zircon are not visible at this scale.

**Figure 3:** Electron microprobe X-ray element maps of blueschist chip E1H3-4b. Black and cooler colours indicate lower concentrations, whereas warmer colours indicates higher concentrations. The maps are not quantitative and the colours scales from different maps do not indicate the same numerical concentrations.

**Figure 4:** a) BSE and X-ray elemental maps of an amphibole grain from the blueschist clast. Dotted white lines indicate the boundary of the core, main grain volume and sharp rim. b) BSE and X-ray elemental maps of a chlorite grain that includes epidote (white core). Dotted line indicates thin outer rim. The maps are not quantitative and the colours scales from different maps do not indicate the same numerical concentrations.

**Figure 5:** Mineral composition plots. a) Amphibole compositions. b) Chlorite compositions. c) Epidote compositions. d) Clinopyroxene compositions.

**Figure 6:** BSE images of locations of rutile and zircon targeted for U–Pb dating by Zack et al. (2013). a) Metamorphic rutile rimming Ti-magnetite, further rimmed by retrograde titanite. b) Zircon in the amphibole matrix. c) Zircon associated with metamorphic allanite/epidote. Ti-mag: Ti-magnetite, Ru: Rutile, Ttn: Titanite, Ep: Epidote, Chl: Chlorite, Amph: Amphibole, Zrc: Zircon, All: Allanite.

**Figure 7:** U–Pb Concordia for a) rutile and b) zircon analyses conducted on blueschist clast sample E1H3-4b. Individual error ellipses (open) and error-weighted averages (filled) are plotted at 95% confidence. Ages are calculated as concordia ages with probabilities of concordance of 0.98 (rutile) and 0.69 (zircon) using Isoplot v.4.15 (Ludwig, 2012).

**Figure 8:** P–T mineral equilibria model for the blueschist chip, bulk composition used is in upper left corner in mol %. a) Mineral equilibria model with inferred P–T path as a grey arrow, dashed line represents unconstrained evolution. Fine black dotted line indicates rutile in and maximum rutile modes. Variance is coloured where v = 6 is the darkest shade and variance decreases as the shade lightens. Purple dashed lines indicate the locations of the omphacite-diopside and actinolite-hornblende solvi. b) Mineral equilibria model with ranges of amphibole compositions A (xNa on the A site), C (xCa on the M4 site) and Z (xNa on the M4 sites) are shown as shaded grey areas, and mineral modes as coloured solid lines.  Chl: chlorite, Amph: Amphibole, O: Omphacite, Di: Diopside, Ep: Epidote, Ru: Rutile, Ttn: Titanite, Act: Actinolite, Gl: Glaucophane, Q: Quartz, Ilm: Ilmenite, Hem: Hematite, Law: Lawsonite, G: Garnet.

**Figure 9:** Pressure–temperature estimates from real subducted rocks and numerical models. Grey arrow indicates the P–T path of this study. a) Real rock dataset of Penniston-Dorland et al. (2015). b) Real rock dataset of Brown and Johnson (2018), including all low temperature-high pressure datasets. c) Real rock dataset of Agard et al. (2018), data from mélanges is indicated as circles. d) Prograde pressure-temperature paths taken from the top of subducting slabs from numerical models of Gerya et al. (2002), Syracuse et al. (2010), van Keken et al. (2011) and Ruh et al (2015).

**Figure 10:** Schematic model for formation and exhumation of the blueschist chip. Structure of subduction zone after Fryer et al. (1999), Oakley et al. (2008) and Pabst et al. (2012). Schematic serpentinisation after Ruh et al (2015). Blueschist clast indicated as purple star. The mechanism of exhumation of the blueschist clast from ca. 50 km ca. 49 Ma ago to the shallow region under the forearc before the last 3 Ma is unknown.

Figure
Click here to download high resolution image

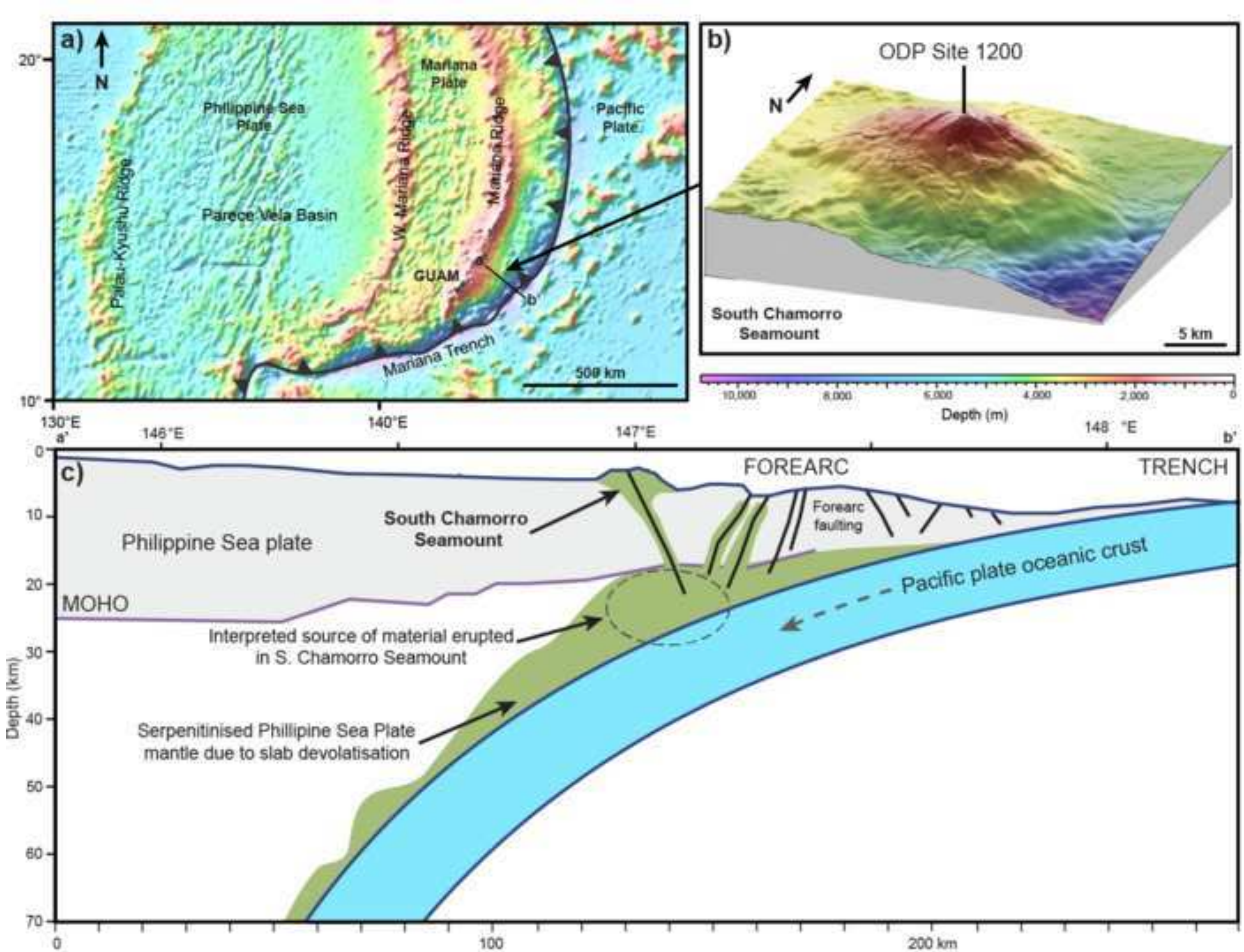

Figure
Click here to download high resolution image

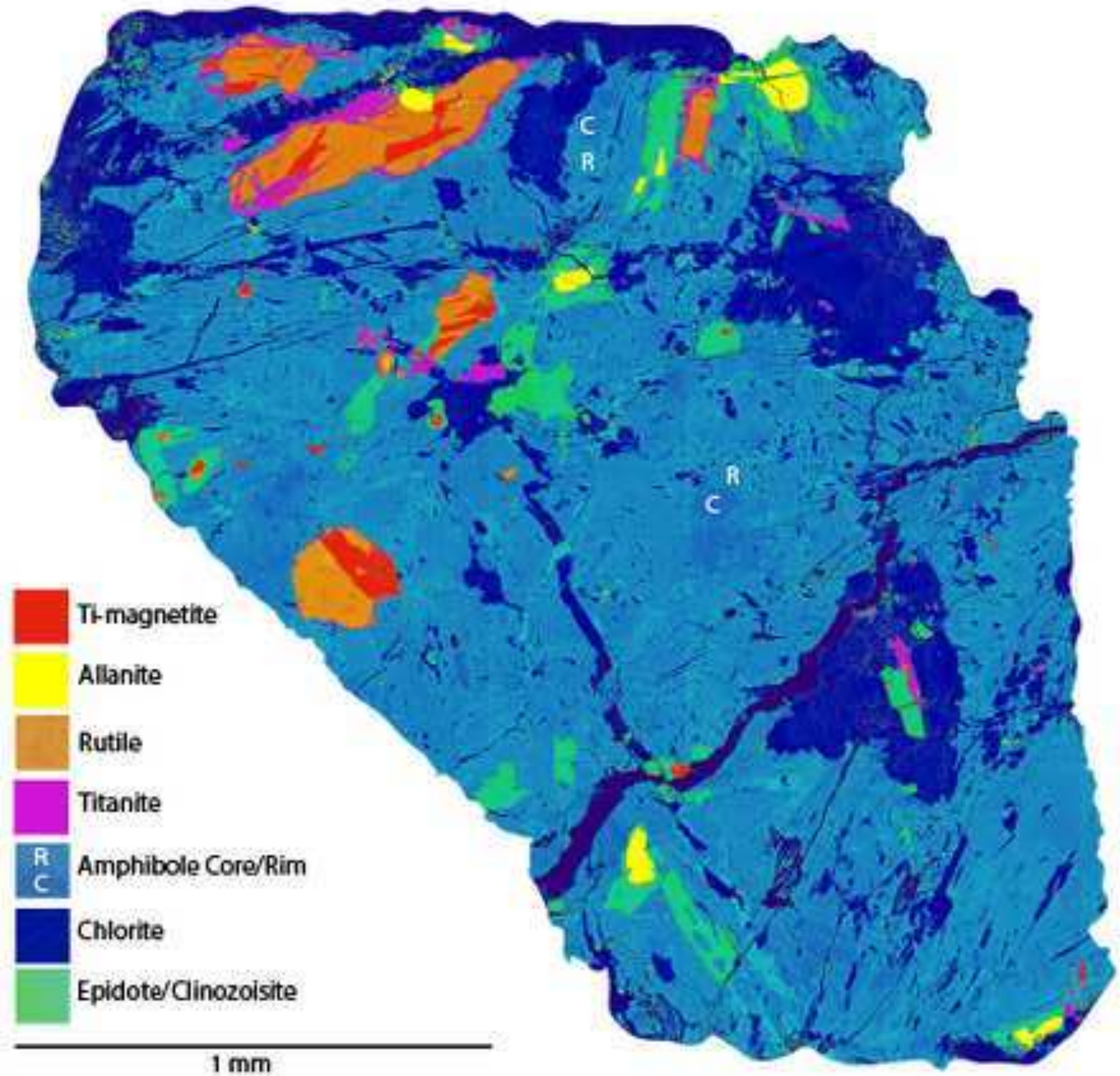

Figure
Click here to download high resolution image

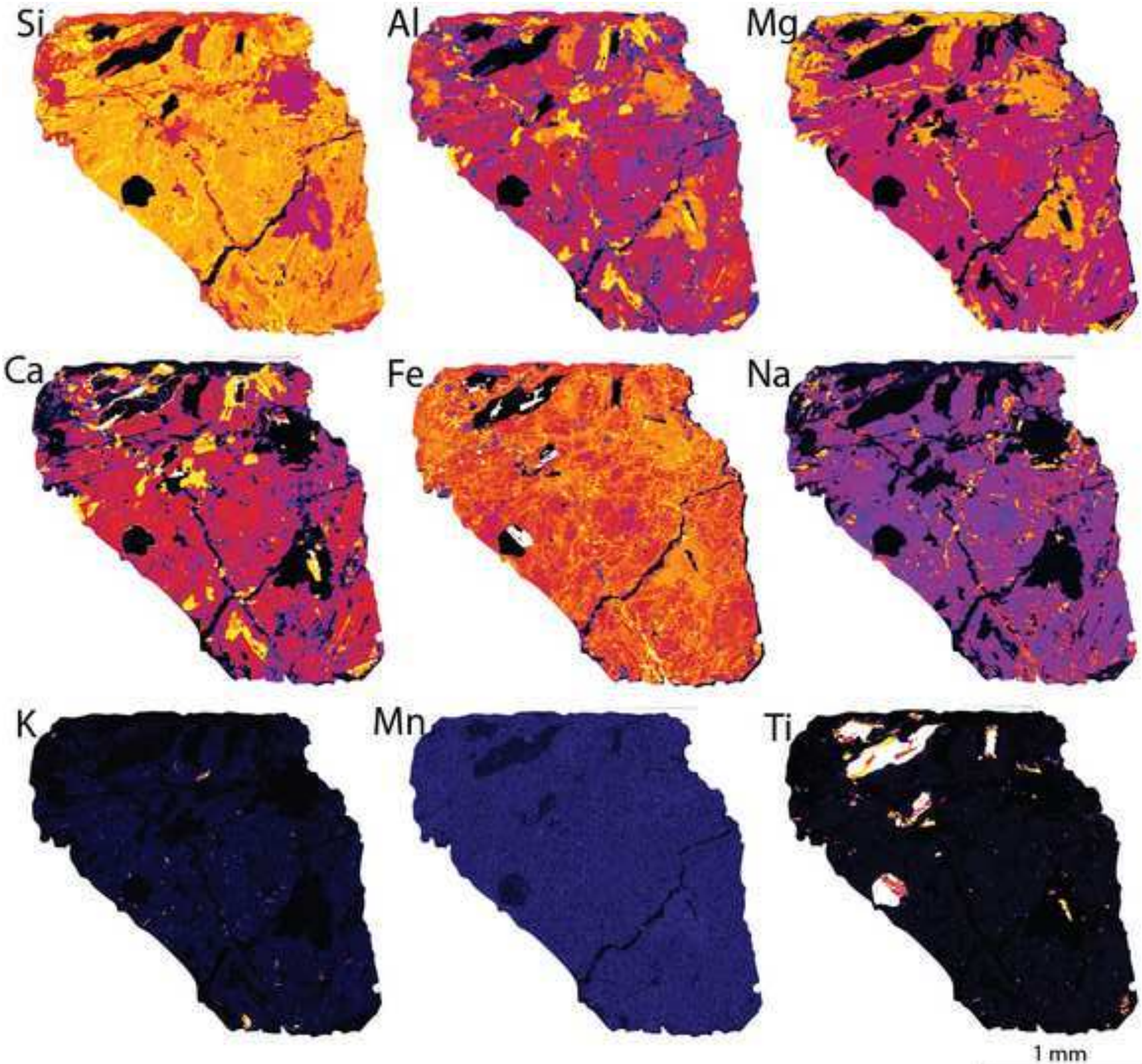

**Figure**

**Click here to download high resolution image**

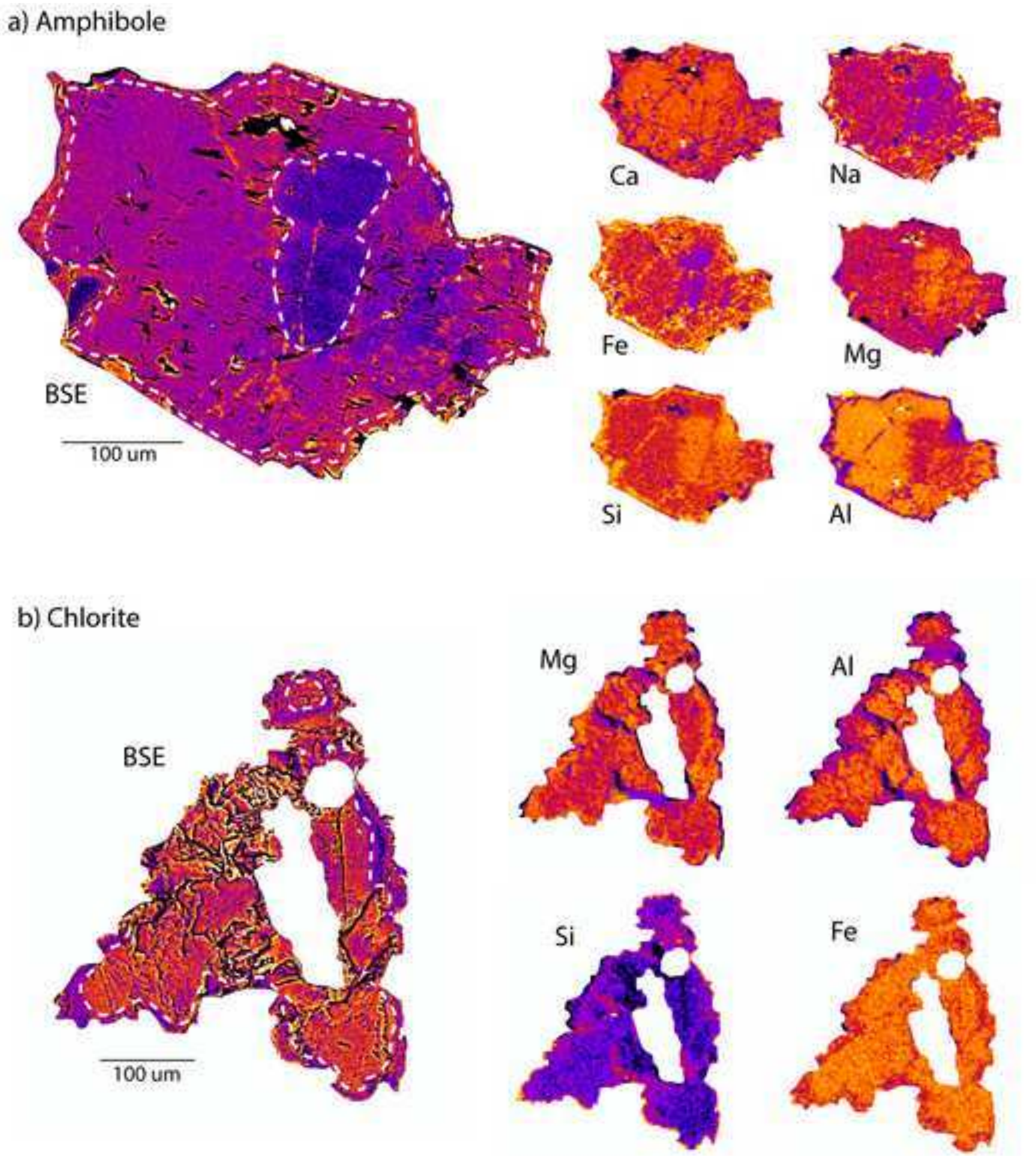

Figure

Click here to download high resolution image

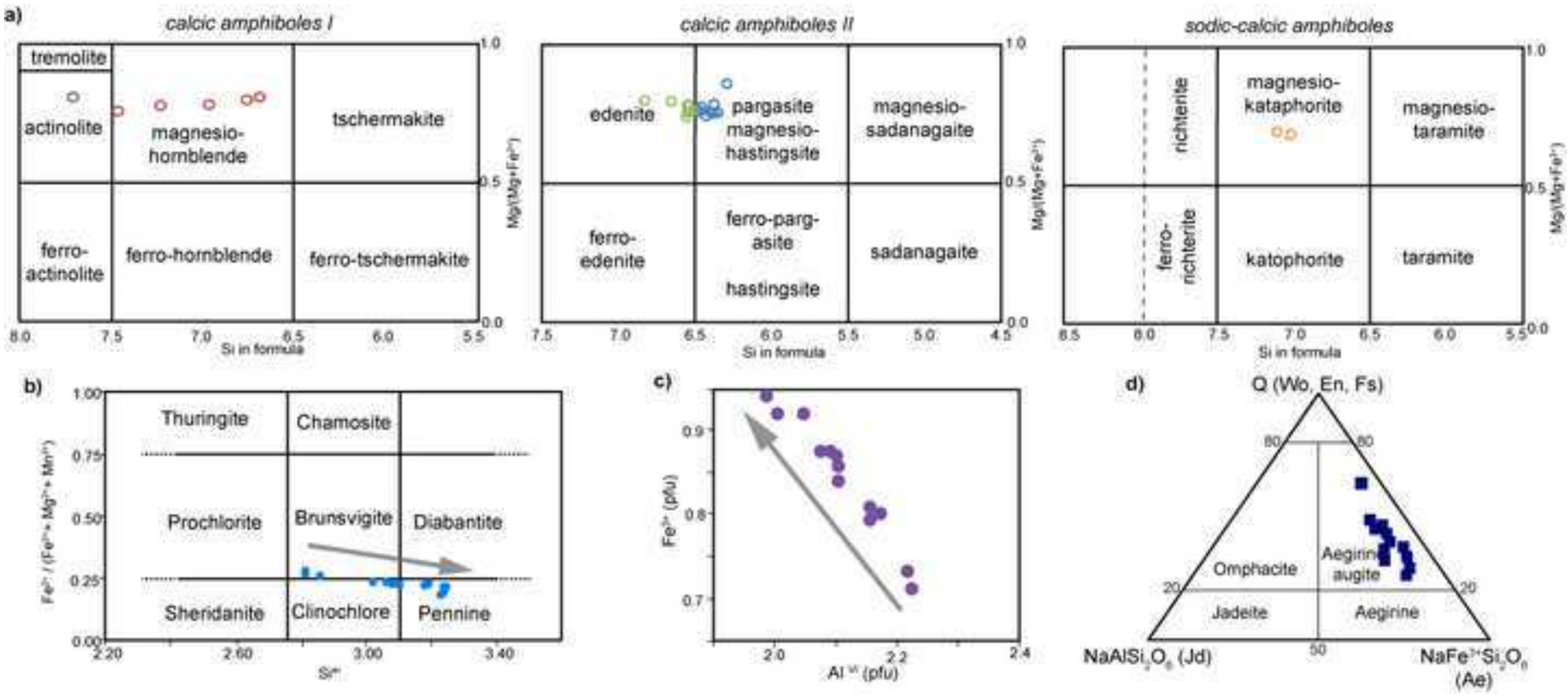

Figure
Click here to download high resolution image

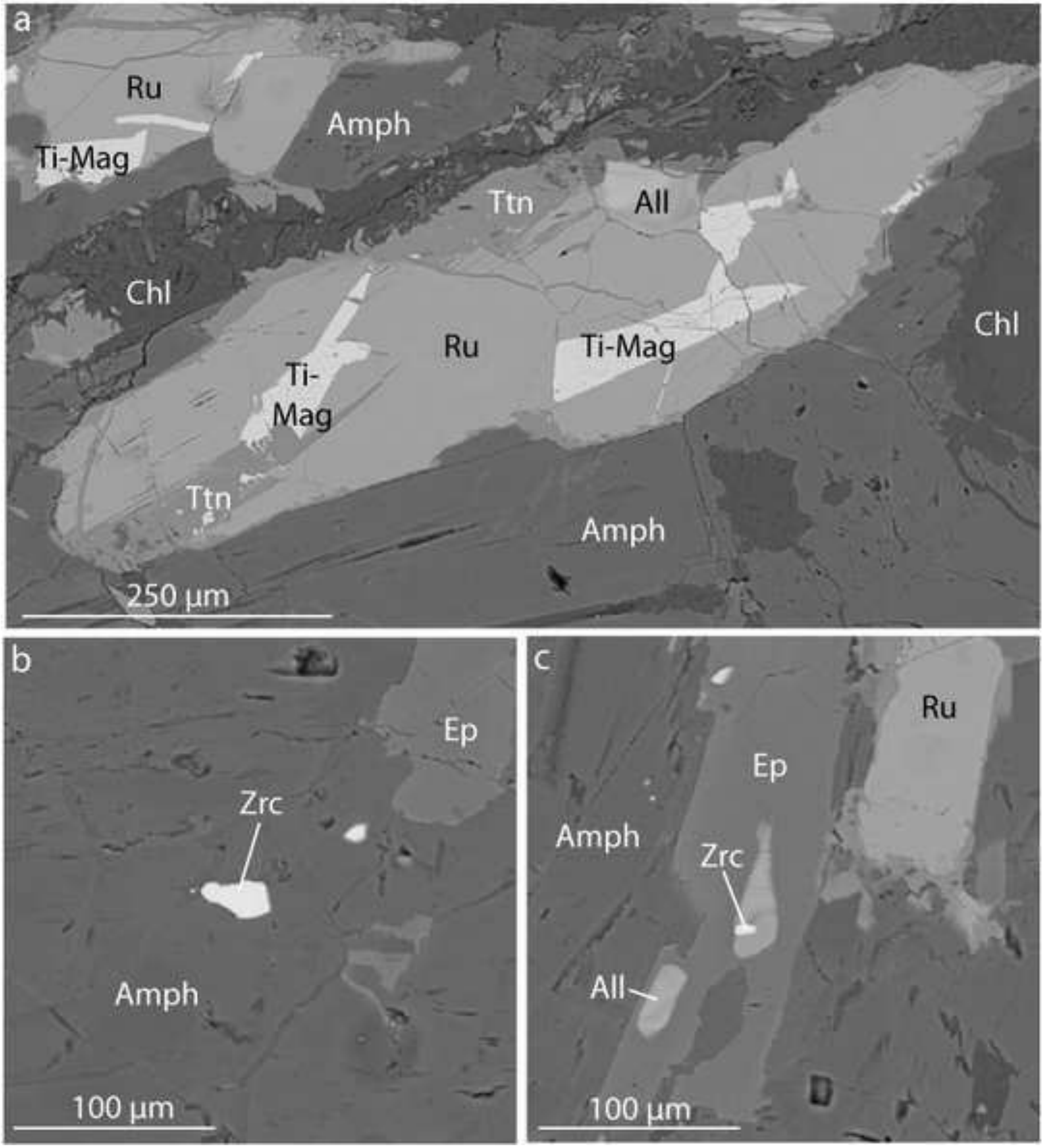

Figure
Click here to download high resolution image

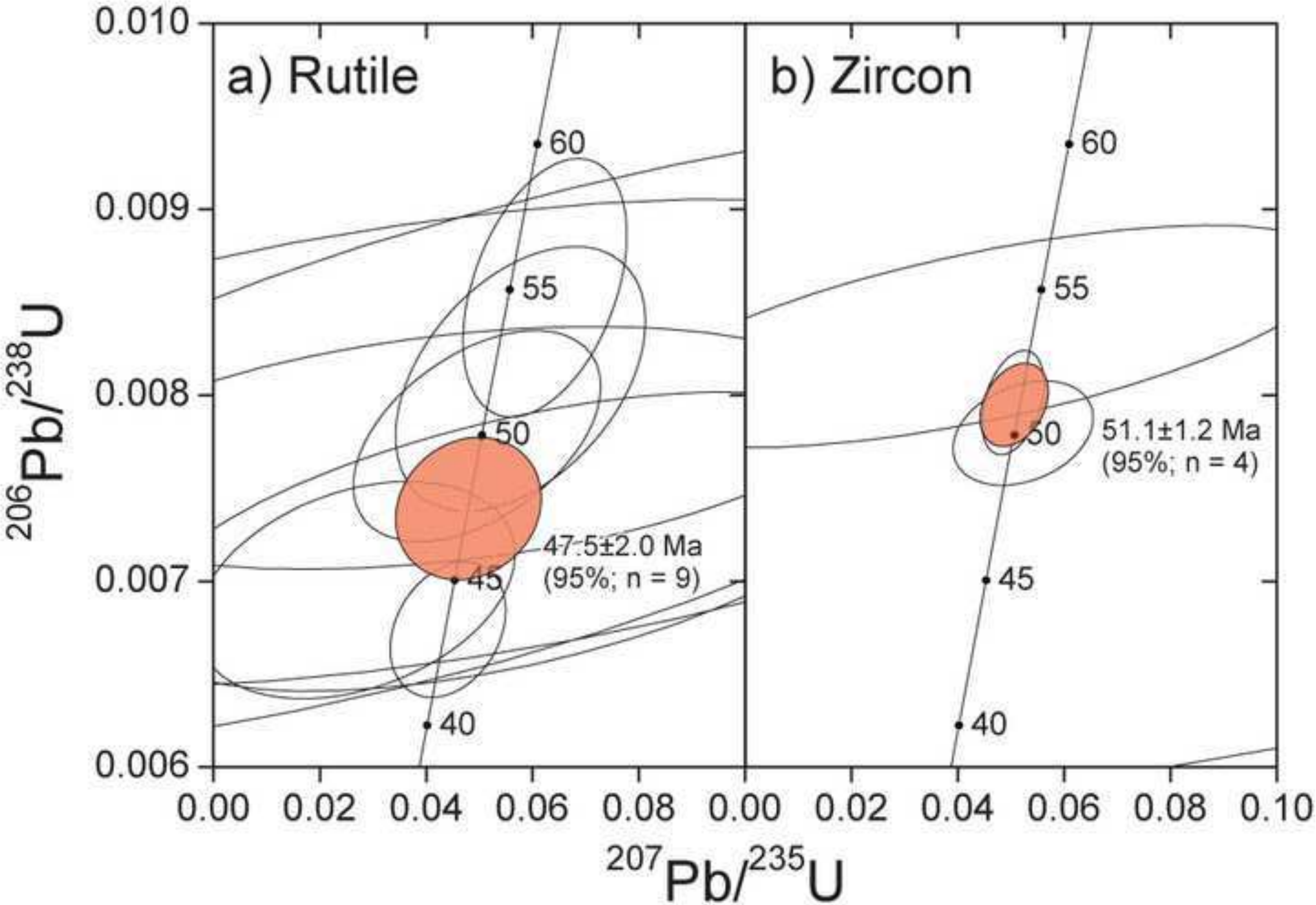

Figure
Click here to download high resolution image

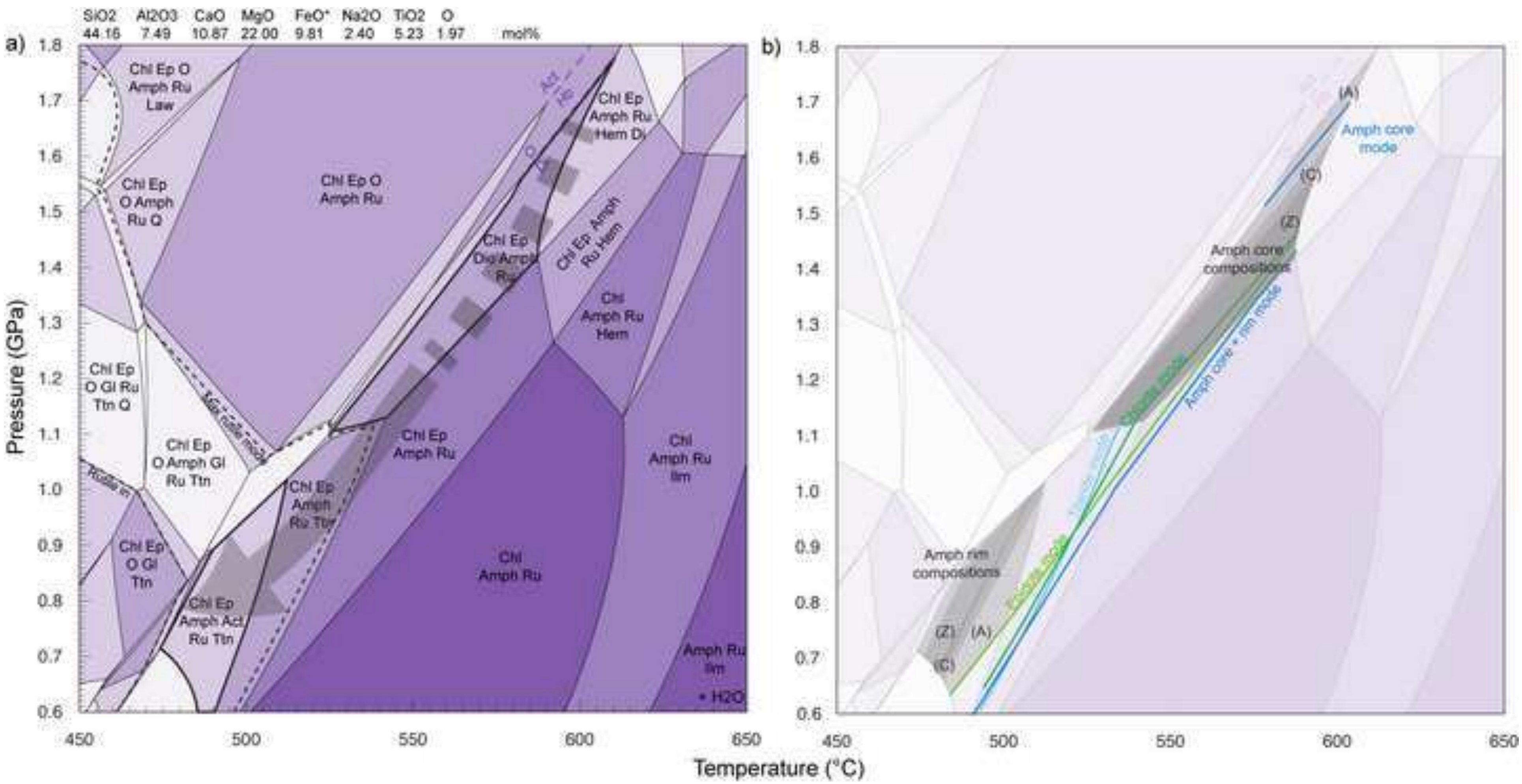

Figure

Click here to download high resolution image

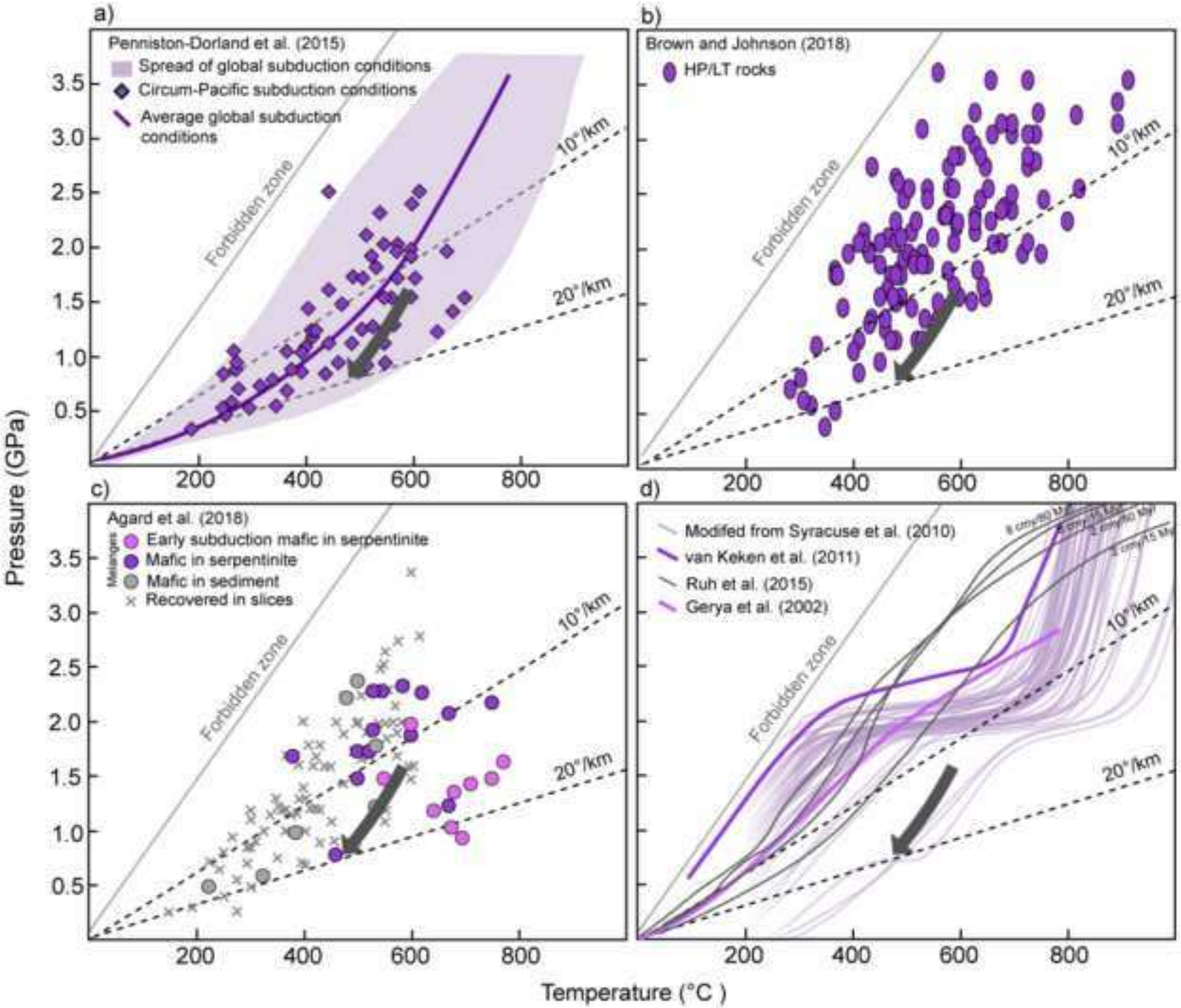

Figure
Click here to download high resolution image